

Improved Transformerless Inverter for PV Grid Connected Power System by using ISPWM Technique

R.Antony Raja Sekar^{#1}, D.Arun Prasad^{*2}

[#]PG Scholar, Department of EEE, PSNA College of Engg & Tech, Dindigul, Tamilnadu, India

^{*}Assistant Professor, Department of EEE, PSNA College of Engg & Tech, Dindigul, Tamilnadu, India

Abstract – This paper presents an improved transformerless inverter with common mode leakage current elimination for a photovoltaic grid connected power system by using inverse sine carrier pulse width modulation (ISPWM). To eliminate the common-mode leakage current in the transformerless photovoltaic grid-connected system, an improved single-phase inverter topology is presented. The improved transformerless inverter can sustain the same low input voltage as the full-bridge inverter and guarantee to eliminating common-mode leakage current. The inverse sine carrier pulse width modulation (ISPWM) control strategy can be applied to implement the presented inverter. The lower total harmonic distortion and higher fundamental output voltage are obtained by using the inverse sine carrier pulse width modulation (ISPWM). The maximum power point tracking (MPPT) is used to extract the maximum power from PV panel. The high efficiency and convenient thermal design are achieved thanks to the decoupling of two additional switches connected to the dc side of the inverter.

Keywords— Photovoltaic (PV) system, Inverse sine carrier pulse width modulation (ISPWM), Improved transformerless inverter, Maximum power point tracking (MPPT).

I. INTRODUCTION

The grid-connected photovoltaic (PV) systems, especially the low-power single-phase systems, call for high efficiency, small size, light weight, and low-cost grid connected inverters. Most of the commercial PV inverters employ either line-frequency or high-frequency isolation transformers. However, line-frequency transformers are large and heavy, making the whole system bulky and hard to install. Topologies with high-frequency transformers commonly include several power stages, which increases the system complexity and reduces the system efficiency [1], [2].

Consequently, the transformerless configuration for PV systems is developed to offer the advantages of small size, high efficiency, high power density, and low cost. Unfortunately, there are some safety issues because a galvanic connection between the grid and the PV array exists in the transformerless systems. A common-mode leakage current flows through the parasitic capacitor between the PV array and the ground [3]. The common-mode leakage current increases the system losses, reduces the grid-connected current quality, induces the severe conducted and radiated

electromagnetic interference, and causes personal safety problems.

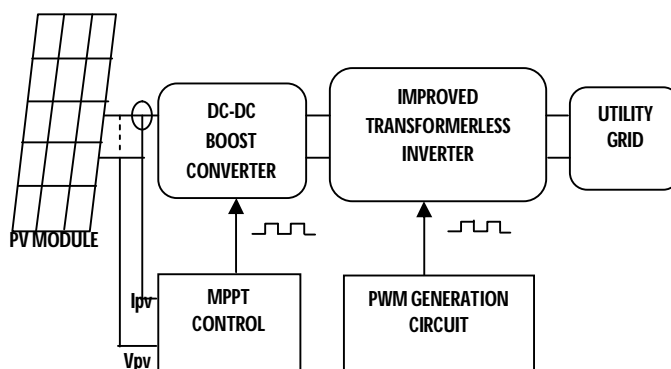


Fig. 1 Overall Block Diagram of the System

The improved transformerless inverter to minimize the common-mode leakage current and improve the efficiency, weight, and size of the whole PV grid-connected power system. In this paper, an improved grid-connected inverter topology for transformerless PV systems is presented, which can sustain the same low input voltage as the full-bridge inverter and guarantee not to generate the common-mode leakage current. Fig. 1 shows the overall block diagram of the system. The inverse sine carrier pulse width modulation (ISPWM) can be applied in the presented inverter. The lower total harmonic distortion and higher fundamental output voltage are obtained by using the inverse sine carrier pulse width modulation (ISPWM) [9]. Therefore, a smaller filter inductor can be employed and the harmonic contents of the output current are reduced greatly, and the grid-connected power quality is improved accordingly.

II. CONDITION OF ELIMINATING THE COMMON-MODE LEAKAGE CURRENT

Without an isolated transformer in the PV grid-connected power systems, there is a galvanic connection between the grid and the PV array, which may form a common-mode resonant circuit and induce the common-mode leakage current. The simplified equivalent model of the common-mode resonant circuit has been derived in as shown in the Fig. 2, where C_{PV} is the parasitic capacitor, L_A and L_B are the filter inductors, i_{cm} is the common-mode leakage current.

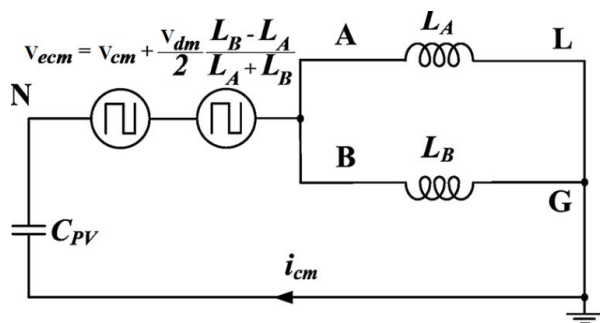


Fig. 2 Simplified Equivalent Model of Common-mode Resonant Circuit
An equivalent common-mode voltage V_{ecm} is defined by

$$V_{ecm} = V_{cm} + \frac{V_{dm} L_B - L_A}{2 L_A + L_B} \quad (1)$$

where V_{cm} is the common-mode voltage, V_{dm} is the differential mode voltage, V_{AN} and V_{BN} are the output voltages of the inverter relative to the negative terminal N of the dc bus as the common reference

$$V_{cm} = \frac{V_{AN} + V_{BN}}{2} \quad (2)$$

$$V_{dm} = V_{AB} = V_{AN} - V_{BN} \quad (3)$$

It is clear that the common-mode leakage current i_{cm} is excited by the defined equivalent common-mode voltage V_{ecm} . Therefore, the condition of eliminating common-mode leakage current is drawn that the equivalent common-mode voltage V_{ecm} must be kept a constant as follows

$$\begin{aligned} V_{ecm} &= V_{cm} + \frac{V_{dm} L_B - L_A}{2 L_A + L_B} \\ &= \frac{V_{AN} + V_{BN}}{2} + \frac{V_{AN} - V_{BN}}{2} \frac{L_B - L_A}{L_A + L_B} \\ &= \text{constant} \end{aligned} \quad (4)$$

One of the filter inductors L_A and L_B is commonly zero. The condition of eliminating common-mode leakage current is accordingly met that

$$\begin{aligned} V_{ecm} &= \frac{V_{AN} + V_{BN}}{2} + \frac{V_{AN} - V_{BN}}{2} = V_{AN} \\ &= \text{constant} (L_A = 0) \end{aligned} \quad (5)$$

$$\begin{aligned} V_{ecm} &= \frac{V_{AN} + V_{BN}}{2} - \frac{V_{AN} - V_{BN}}{2} = V_{BN} \\ &= \text{constant} (L_B = 0) \end{aligned} \quad (6)$$

As a result, the condition of eliminating common-mode leakage current is met that

$$\begin{aligned} V_{ecm} &= V_{cm} = \frac{V_{AN} + V_{BN}}{2} \\ &= \text{constant} (L_A = L_B) \end{aligned} \quad (7)$$

III. ISPWM TECHNIQUE

The modulation strategy employed in this paper is the inverted sine PWM (ISPWM) technique. In the conventional PWM method, triangular wave is used as carrier wherein they are replaced by inverted sine carrier waves in this model in Fig. 3.

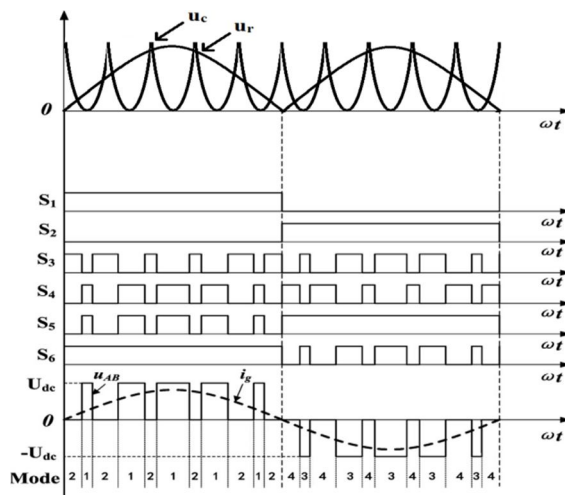


Fig . 3 Generation of pulse using ISPWM

The inverse sine carrier pulse width modulation (ISPWM) technique has a better spectral quality and a higher fundamental component compared to the conventional sinusoidal PWM without any pulse dropping. Also, there is a reduction in the total harmonic distortion (THD).

An inverted sine wave of high switching frequency is taken as a carrier wave and is compared with that of the reference sine wave. The pulses are generated whenever the amplitude of the reference sine wave is greater than that of the inverted sine carrier wave [10]. PIC microcontroller is used to obtain the gating pattern for the individual IGBTs. The total harmonic distortion for the different values of switching frequencies is obtained and is found to be lesser than the conventional method. By employing this new modulation technique it has been proved that the fundamental voltage is improved throughout the working range and is greater than the voltage obtained using conventional method which employs triangular carriers for modulation.

IV. BOOST CONVERTER AND MAXIMUM POWER POINT TRACKING

The boost converter has one controlled semiconductor switch and it is controlled by applying appropriate gating pulses. The turn off resistance of the switch is very much higher than the turn on resistance. Thus by varying the duty cycle of the gating pulse, the effective resistance offered by the circuit is varied.

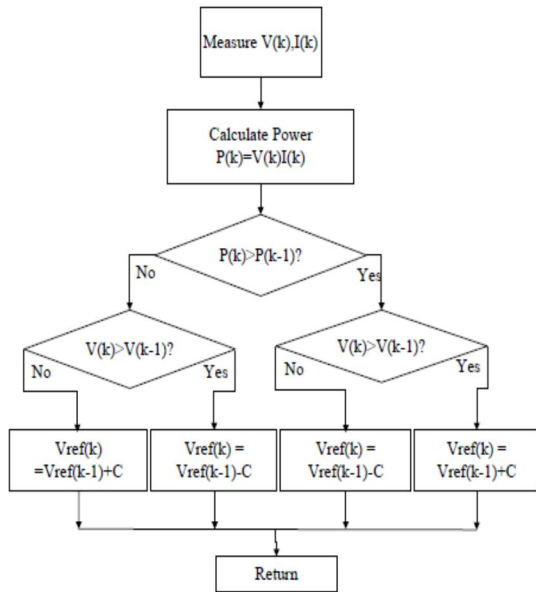


Fig. 4 Flow Chart of P&O Algorithm

The boost converter is placed right between the inverter and the PV panel to ensure maximum power transfer. The resistance of the circuit as seen from the PV panel must be equal to the internal resistance of the PV module for maximum power transfer. The duty cycle of the boost converter is adjusted in such a way that maximum power is transferred from the module to the output terminal.

The performance of the PV panel depends highly on the environmental conditions which vary throughout the day. The efficiency of the PV panel is very less and hence it becomes necessary to extract the maximum power from the panel by shifting the operating point to the maximum power point. The operating point of the PV panel is fixed by the load resistance. Perturb and observe (P&O) algorithm is adopted in this work due to its simplicity. In this algorithm, a perturbation is made on the PV panel operating point to force tracking in the direction towards maximum power point [7]. The flowchart of the P&O algorithm is shown in Fig.4.

The voltage and current of the PV panel are measured after one perturbation and the power is calculated. This is then compared with the previous value of power and the difference ΔP ($\Delta P = P_k - P_{k-1}$) is calculated. If ΔP is positive, perturbation is continued in the same direction. For negative values of ΔP , the direction of perturbation is reversed.

V. IMPROVED TRANSFORMERLESS INVERTER TOPOLOGY

Fig. 5 shows the improved grid-connected inverter topology, which can meet the condition of eliminating common-mode leakage current. In this topology, two additional switches S5 and S6 are symmetrically added to the conventional full-bridge inverter, and the inverse sine carrier pulse width modulation strategy applied to the inverter and output can be achieved.

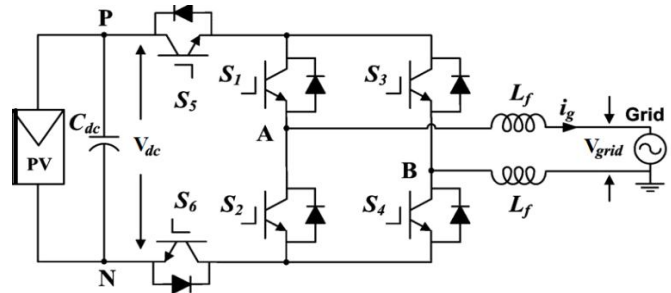


Fig. 5 Improved Transformerless Inverter Topology

The full- bridge inverter with inverse sine carrier pulse width modulation, the improved inverter has one phase leg including S1 and S2 operating at the grid frequency, and another phase leg including S3 and S4 commutating at the switching frequency. Two additional switches S5 and S6 commute alternately at the grid frequency and the switching frequency to achieve the dc-decoupling states. Accordingly, four operation modes that generate the voltage states of +Vdc, 0, -Vdc are shown in Fig. 6.

A. Operating Modes of Improved Transformerless Inverter

Mode 1: when S4 and S5 are ON, $V_{AB} = +V_{dc}$ and the inductor current increases through the switches S5, S1, S4, and S6.

The common-mode voltage is

$$V_{cm} = \frac{1}{2} (V_{AN} + V_{BN}) = \frac{1}{2} (V_{dc} + 0) = \frac{V_{dc}}{2} \quad (8)$$

Mode 2: when S4 and S5 are turned OFF, the voltage V_{AN} falls and V_{BN} rises until their values are equal, and the antiparallel diode of S3 conducts. Therefore, $V_{AB} = 0V$ and the inductor current decreases through the switch S1 and the antiparallel diode of S3.

The common-mode voltage changes into

$$V_{cm} = \frac{1}{2} (V_{AN} + V_{BN}) = \frac{1}{2} \left(\frac{V_{dc}}{2} + \frac{V_{dc}}{2} \right) = \frac{V_{dc}}{2} \quad (9)$$

Mode 3: when S3 and S6 are ON, $V_{AB} = -V_{dc}$ and the inductor current increases reversely through the switches S5, S3, S2, and S6.

The common-mode voltage becomes

$$V_{cm} = \frac{1}{2} (V_{AN} + V_{BN}) = \frac{1}{2} \left(0 + \frac{V_{dc}}{2} \right) = \frac{V_{dc}}{2} \quad (10)$$

Mode 4: when S3 and S6 are turned OFF, the voltage V_{AN} rises and V_{BN} falls until their values are equal, and the antiparallel diode of S4 conducts. Similar as to Mode 2, $V_{AB} = 0V$ and the inductor current decreases through the switch S2

and the antiparallel diode of S4 . The common-mode voltage V_{cm} also keeps $V_{dc}/2$ referring to (9). From (8) to (10) the common-mode voltage can remain a constant $V_{dc}/2$ during the four commutation modes in the improved inverter with inverse sine carrier pulse width modulation.

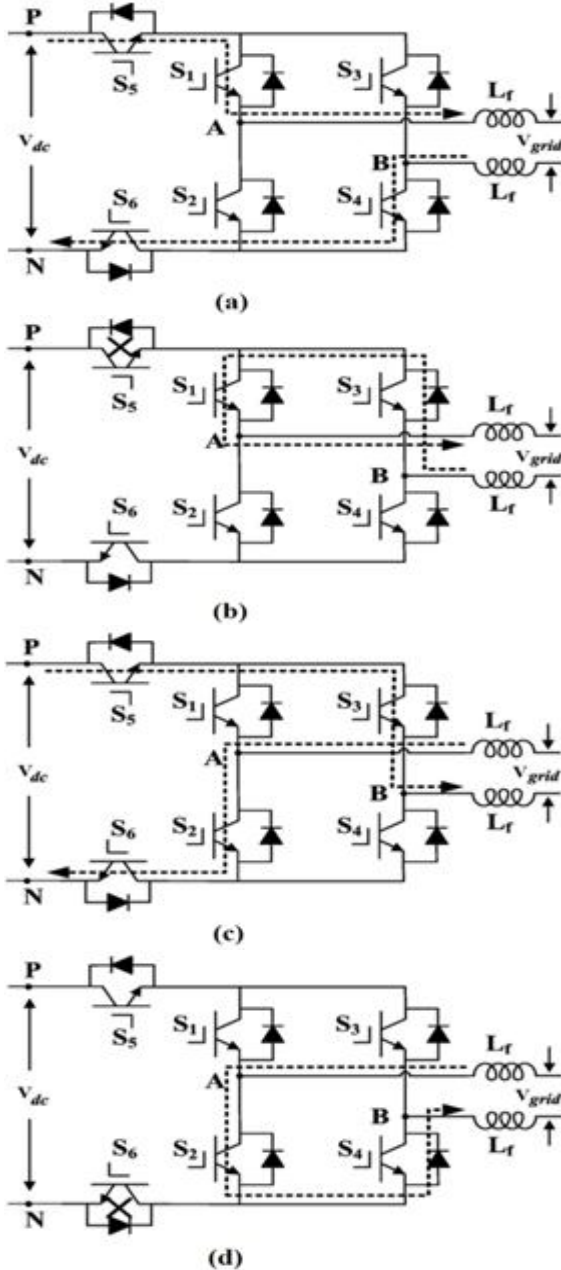


Fig. 6 Modes of Operation of the Improved Transformerless Inverter with ISPWM (a) Mode 1. (b) Mode 2. (c) Mode 3. (d) Mode 4.

B. Simulation and Waveforms

In order to verify the theoretical analysis in previous sections, The system is simulated, having the frame of the panels connected to ground with the parasitic capacitance of 75 nF. The detailed components and parameters used are as follows: input voltage, $V_{dc} = 220V$; input capacitor, $C_{dc} = 940 \mu F$; grid voltage, $U_g = 220V_{ac}$; grid frequency, $f_g = 50 \text{ Hz}$;

switch frequency, $f_s = 20 \text{ kHz}$; filter inductor, $L_f = 4 \text{ mH}$; parasitic capacitor, $CPV = 75 \text{ nF}$; power switches, S1–S6 = IRGB4056DPbF; junction capacitors of the switches, C1–C5 : 29 pF.

TABLE I
PARAMETERS OF IMPROVED TRANSFORMERLESS INVERTER TOPOLOGY

SI.no	Parameter	Value
1	Input voltage, V_{dc}	220 V
2	Input capacitor, C_{dc}	940 μF
3	Filter inductor, L_f	1 mH
4	Parasitic capacitor, CPV	75 nF
5	Power switches, S1-S6	IRGB4056DPbF
6	Junction capacitors of the switches, C1–C5	29 pF
7	Grid voltage, U_g	220 V
8	Grid frequency, f_g	50 Hz
9	Switch frequency, f_s	20 kHz

The simulated results by employing the inverse sine carrier pulse width modulation when the junction capacitances of six switches are equal. Fig. 8 shows the Simulation Diagram of Improved Transformerless Inverter for PV Grid Connected System. The input DC voltage is applied to the improved transformerless inverter. The inverter converted the DC supply to AC supply. This AC supply is filtered by the inductor. This filter output AC supply is connected to the grid. The six switches are control in the inverse sine carrier pulse width modulation.

1) Improved Transformerless Inverter Output Voltage:

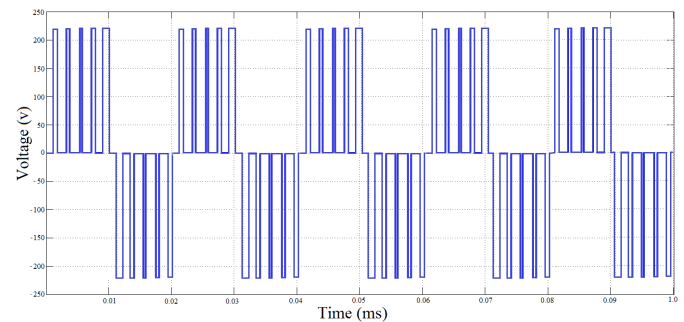


Fig. 7 Output Voltage of Improved Transformerless Inverter by ISPWM

2) Grid Voltage:

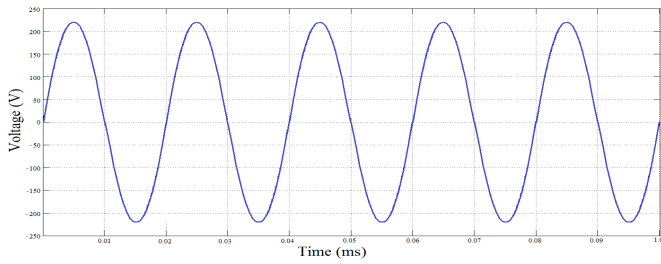


Fig. 8 Grid Voltage (V_g)

3) Grid Current:

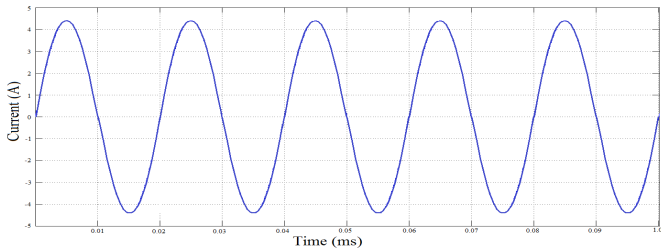


Fig. 9 Grid Current (i_g)

Fig. 7 shows the Output Voltage of Improved Transformerless Inverter by ISPWM. The 220V output voltage is taken from the inverter. Fig. 8 shows the Grid Voltage (V_g). Fig. 9 shows the Grid Current (i_g). The grid current waveform is sinusoidal. The harmonics is low. The leakage ground current is high value in inverter. Fig. 10 shows the Leakage Ground Current of the Normal Transformerless Inverter. Fig. 11 shows the Leakage Ground Current of the Improved Transformerless Inverter. Fig. 12 shows the Harmonic Profile by Unipolar Sinusoidal PWM. Fig. 13 shows the Harmonic Profile by Inverse Sine Carrier PWM.

4) Leakage Ground Current of the Normal Transformerless Inverter:

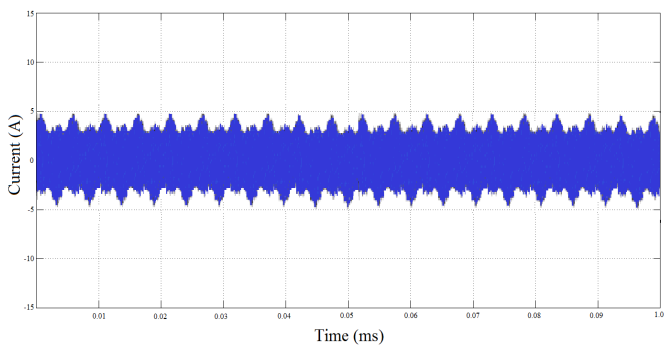


Fig. 10 Leakage Ground Current of the Normal Transformerless Inverter

5) Leakage Ground Current of the Improved Transformerless Inverter:

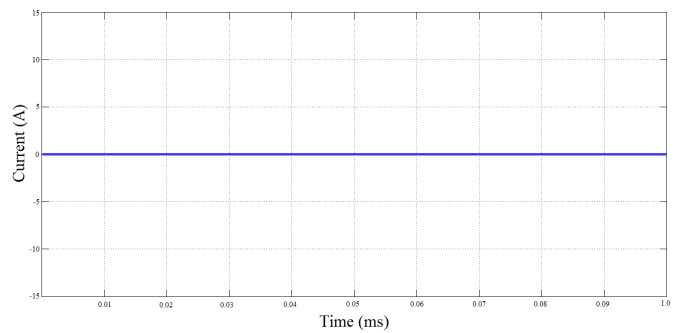


Fig. 11 Leakage Ground Current of the Improved Transformerless Inverter

Therefore, to accord with the value principle of the junction capacitors under the inverse sine carrier pulse width modulation, two additional capacitors with the values of 29 pF are, respectively, paralleled to S3 and S4. It is clear that the grid-connected current is highly sinusoidal synchronized with the grid voltage by achieving the output. The common-mode leakage ground current is almost zero since V_{AN} and V_{BN} are fully complementary in the switching periods. The common-mode leakage ground current i_{cm} is successfully limited within a very small value. The total harmonic distortion (THD) is lower value from the inverse sine carrier pulse width modulation. As it can be seen, the proposed ISPWM technique has always lower THD than the conventional SPWM. The high grid connected current quality is obtained in the system. The fundamental output voltage is higher than the unipolar sinusoidal pulse width modulation. It has a better spectral quality and a higher fundamental component compared to the conventional sinusoidal PWM (SPWM) without any pulse dropping.

By employing this new technique it has been proved that the fundamental voltage is improved throughout the working range and is greater than the voltage obtained using unipolar sinusoidal pulse width modulation. The inverse sine carrier pulse width modulation is applied improve the performance of the inverter. The capability of ISPWM scheme for improving frequency spectrum.

6) Harmonic Profile by Unipolar Sinusoidal PWM:

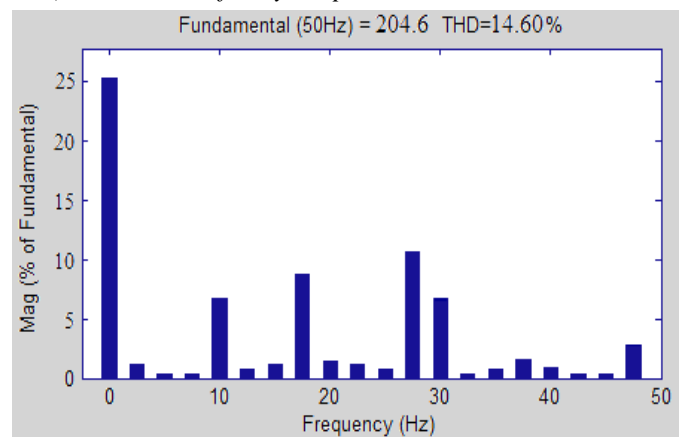


Fig. 12 Harmonic Profile by Unipolar Sinusoidal PWM

7) Harmonic Profile by Inverse Sine Carrier PWM:

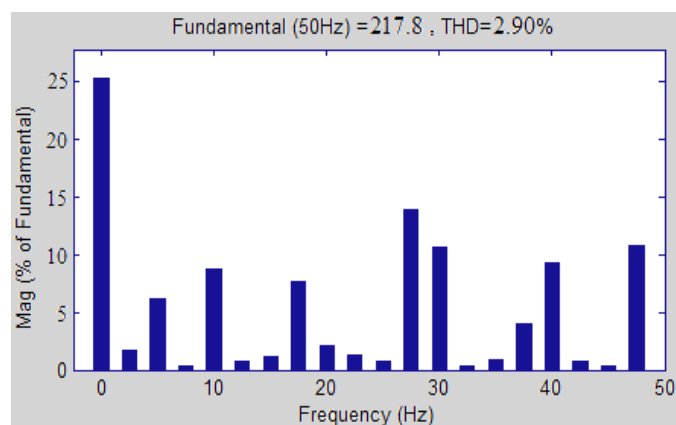


Fig. 13 Harmonic Profile by Inverse Sine Carrier PWM

In addition to this, switching losses and THD are also lower compared to the conventional PWM technique. The maximum power point tracking(MPPT) is used to extract the maximum power from the PV panel.

VI. CONCLUSION

This paper presented an improved grid-connected inverter topology for transformerless PV systems. The inverse sine carrier pulse width modulation control strategy can be applied to implement the presented inverter, which can guarantee not to generate the common-mode leakage current because the condition of eliminating common-mode leakage current is met completely. The high efficiency and convenient thermal design are achieved thanks to the decoupling of two additional switches connected to the dc side of the inverter. Moreover, the lower total harmonic distortion(THD) and higher fundamental output voltage are obtained by inverse sine carrier pulse width modulation(ISPWM). The smaller filter inductors are employed and the copper losses and core losses are reduced accordingly.

VII. REFERENCES

- [1] S.B. Kjaer, J.K. Pedersen, and F. Blaabjerg, "A review of single phase grid - connected inverters for photovoltaic modules," IEEE Trans. Ind., vol. 41, no. 5, pp. 1292-1306, Sep./Oct. 2005.
- [2] Q. Li and P. Wolfs, "A review of the single phase photovoltaic Module Integrated converter topologies with three different DC link configurations," IEEE Trans. Power Electron., vol. 23, no. 3, pp. 1320-1333, May 2008.
- [3] T. Kerekes, R. Teodorescu, and U. Borup, "Transformerless photovoltaic inverters connected to the grid," in Proc. IEEE 22nd Annu. Appl. Power Electron. Conf., 2007, pp. 1733-1737.
- [4] O. Lopez, R. Teodorescu, and J. Doval-Gandoy, "Multilevel Transformerless topologies for single-phase grid-connected converters," in Proc. 32nd Annu. Conf. IEEE Ind. Electron. Soc., Nov. 2006, pp. 5191-5196.
- [5] R. Gonzalez, E. Gubia, J. Lopez, and L. Marroyo, "Transformerless single phase multilevel-based photo voltaic inverter," IEEE Trans. Ind Electron., vol. 55, no. 7, pp. 2694-2702, Jul. 2008.
- [6] T. Kerekes, M. Liserre, R. Teodorescu, C. Klumpner, and M. Sumner, "Evaluation of three-phase transformerless photovoltaic inverter topologies," IEEE Trans. Power Electron., vol. 24, no. 9, pp. 2202-2211, Sep. 2009.
- [7] Vafaoui., B. Wu and R. Cheung, "Implementation of maximum power point tracking algorithm for residential photovoltaic

systems," 2nd Canadian Solar Buildings Conference Calgary, June 10-14, 2007.

- [8] Joe-Air Jiang, Tsong-Liang Huang, Ying-Tung Hsiao, Chia-Hong Chen, "Maximum Power Tracking for Photovoltaic Power Systems," Tamkang Journal of Science and Engineering, 2005, Vol. 8, No. 2, pp. 147-153.
- [9] S. Jeevananthan, R. Nandhakumar, P. Dananjayan, "Inverted Sine carrier for Fundamental Fortification in PWM Inverters and FPGA Based Implementations," Vol.4, No.2, November 2007, 171-187.
- [10] R. Seyezhai, Dr.B.L. Mathur, "Performance Evaluation Of Inverted Sine PWM Technique For An Asymmetric Cascaded Multilevel Inverter," Journal of Theoretical and Applied Information Technology 2009.